Seasonal Prediction Skill of East Asian Summer Monsoon in CMIP5-Models

Bo Huang, Ulrich Cubasch, Christopher Kadow*

Institute of Meteorology, Freie Universität Berlin,
Carl-Heinrich-Becker-Weg 6-10, 12165 Berlin, Germany

Corresponding Author: huangb@live.com

ABSTRACT

The East Asian summer monsoon (EASM) is an important part of the global climate system and plays a vital role in the Asian climate. Its seasonal predictability is a long-standing issue within the monsoon scientist community. In this study, we analyse the seasonal (the leading time is at least six months) prediction skill of the EASM rainfall and its associated general circulation in non-initialised and initialised simulations for the years 1979-2005 which are performed by six prediction systems (*i.e.*, the BCC-CSM1-1, the CanCM4, the GFDL-CM2p1, the HadCM3, the MIROC5 and the MPI-ESM-LR) from the Coupled Model Intercomparison Project phase 5 (CMIP 5). We find that most prediction systems simulated zonal wind over 850 and 200 hPa are significantly improved in the initialised simulations compared to non-initialised simulations. Based on the knowledge that zonal wind indices can be used as potential predictors for the EASM, we select an EASM index based upon the zonal wind over 850 hPa for further analysis. This assessment shows that the GFDL-CM2p1 and the MIROC5 added prediction skill in simulating the EASM index with initialisation, the BCC-CSM1-1, the CanCM4, and the MPI-ESM-LR changed the skill insignificantly, and the HadCM3 indicates a decreased skill score. The different response to the initialisation can be traced back to the ability of the models to capture the ENSO (El Niño-Southern Oscillation)-EASM coupled mode, particularly the Southern Oscillation-EASM coupled mode. As it is known from observation studies, this mode links the oceanic circulation and the EASM rainfall. Overall, the GFDL-CM2p1 and the MIROC5 are capable to predict the EASM on a seasonal time-scale under the current initialisation strategy.

Key Words: East Asian summer monsoon; initialisation; seasonal prediction; ENSO-EASM coupled mode; CMIP5

1. INTRODUCTION

The Asian monsoon is the most powerful monsoon system in the world due to the thermal contrast between the Eurasian continent and the Indo-Pacific Ocean. Its evolution and variability critically influence the livelihood and the socio-economic status of over two billion people who live in the Asian monsoon dominated region. It encompasses two sub-monsoon systems, the South Asian monsoon (SAM) and the East Asian monsoon (EAM) (Wang, 2006). In summer time (June-July-August), the EAM, namely, the East Asian summer monsoon (EASM) occurs from the Indo-China peninsula to the Korean Peninsula and Japan, and shows strong intraseasonal-to-interdecadal variability (Ding and Chan, 2005). Thus, an accurate prediction of the EASM is an important and long-standing issue in climate science.

To predict the EASM, there are two approaches, statistical prediction and dynamical prediction, respectively. The statistical method seeks the relationship between the EASM and a strong climate signal (e.g., ENSO, NAO; Wu et al., 2009;Yim et al., 2014;Wang et al., 2015). This method establishes an empirical equation between the EASM and climate index. However, it is limited by the strength of the climate signal. The other method is dynamical prediction. It employs a climate model to predict the EASM (Sperber et al., 2001;Kang and Yoo, 2006;Wang et al., 2008a;Yang et al., 2008;Lee et al., 2010;Kim et al., 2012). Without initialisation, both the atmosphere general circulation models (AGCMs) and the coupled atmosphere-ocean general circulation models (CGCMs) cannot predict the climate on seasonal time-scale (Goddard et al., 2001). Given an initial condition, the AGCMs have the ability to predict the climate, but show little skill in predicting the EASM (Wang et al., 2005;Barnston et al., 2010). Because the AGCMs fail to produce a correct relationship between the EASM and the sea surface temperature (SST) anomalies over the tropical western North Pacific, the South China Sea, and the Bay of Bengal (Wang et al., 2004;Wang et al., 2005), the monsoon community endeavours to predict the EASM with CGCMs (Wang et al., 2008a;Zhou et al., 2009;Kim et al., 2012;Jiang et al., 2013).

CGCMs have proved to be the most valuable tools in predicting the EASM (Wang et al., 2008a;Zhou et al., 2009;Kim et al., 2012;Jiang et al., 2013). However, the performance of CGCMs in predicting the EASM on seasonal time-scale strongly depends on their ability to reproduce the air-sea coupled process (Kug et al., 2008) and on the given initial condition (Wang et al., 2005). In the coupled model inter-comparison project (CMIP) phase 3 (CMIP3;

Meehl et al., 2007) era, the models simulate, not only a too weak tropical SST-monsoon teleconnection (Kim et al., 2008;Kim et al., 2011), but also a too weak East Asian zonal wind-rainfall teleconnection (Sperber et al., 2013). Compared to CMIP3 models, CMIP phase 5 (CMIP5; Taylor et al., 2012) models improve the representation of monsoon status (Sperber et al., 2013). Therefore, given the initial conditions, the CMIP5 models do have the potential to predict the EASM.

As mentioned, initial conditions do play a vital factor in predicting the EASM on sub-seasonal to seasonal time-scale (Wang et al., 2005;Kang and Shukla, 2006). Under the current set up of initialisation, the CMIP5 models show the ability to predict the SST variation index (*i.e.*, El Niño-Southern Oscillation-ENSO index; Niño3.4) of up to 15 months in advance (Meehl and Teng, 2012;Meehl et al., 2014;Choi et al., 2016). This extended prediction skill of the ENSO suggests that the EASM can be predicted on a seasonal time-scale if the dynamical link between the ENSO and monsoon circulations is well represented in these models. Two scientific questions will be addressed in this study: 1. How realistic are the initialised CMIP5 models in representing the EASM? 2. Can the CMIP5 models capture the dynamical link between the ENSO and EASM?

In this paper, we will intercompare the influence of the initialisation on the capability of the CMIP5 models to capture the EASM and the ENSO-EASM teleconnections. The model simulations, comparison data and methods are introduced in Section 2. Section 3 describes the seasonal skill of the rainfall predictions and the prediction of the associated general circulation of the EASM. The mechanism causing the differential response of the models to the initialisation is presented in Section 4. The discussions are shown in Section 5. Section 6 summarises the findings of this paper.

2. MODELS, DATA AND METHODS

2.1 MODELS AND INITIALISATION

In this study, we evaluate six prediction systems from CMIP5 project (Table 1), which have performed a yearly initialisation (Meehl et al., 2014). Their simulations can be used in seasonal prediction study. There are two group of experiments, without initialisation (non-initialisation) and with initialisation, respectively. For non-initialised simulations, the models are forced by observed atmospheric composition changes (reflecting both anthropogenic and natural sources) and, for the first time, including the time-evolving land cover (Taylor et al., 2012). For initialised simulations, the models update the time-evolving observed atmospheric

and oceanic component (Taylor et al., 2012). Following the CMIP5 framework, the six models establish their initialisation strategy, which are summarised in Table 2. More details about the initialisation strategy of each model can be found in the reference paper in Table 1. To simplify the comparison, we select the first lead year (up to 12 months) results for further analysis. The HadCM3-ff is the full-field initialised simulation, which employs the same CGCM (HadCM3) as the anomaly initialisation. Satellite era (1979 to 2005) simulations are used in the study due to the spatial coverage of precipitation observations.

The six models employ different initialisation strategies for atmospheric and oceanic process, and for initial date (Table 2). These initialisation strategies contribute to a new approach for climate prediction on decadal time-scale (Meehl et al., 2014). As the ocean is driving the long-term prediction skill rather than the initial condition of the atmosphere, the timing of the initialization has to be considered in the time scale of the ocean circulation, i.e. years to decades. Therefore, on an ocean time scale, the initialization takes place with comparable timing and therefore the results are comparable. This approach based on decadal prediction experiments, which deviates from the scores of other seasonal prediction experiments based on initialisation techniques derived from weather forecasting.

2.2 COMPARISON DATA

The main datasets which are used for comparison in this study include: (1) monthly precipitation data from the Global Precipitation Climatology Project (GPCP; Adler et al., 2003); (2) monthly circulation data from ECMWF Interim re-analysis (ERA-Interim; Dee et al., 2011); and (3) monthly mean SST from National Oceanic and Atmospheric Administration (NOAA) improved Extended Reconstructed SST version 4 (ERSST v4; Huang et al., 2015). All the model data and the comparison data are remapped onto a common grid of 2.5ºx2.5º by bi-linear interpolation to reduce the uncertainty induced by different data resolutions.

2.3 EAST ASIAN MONSOON INDEX AND ENSO INDEX

In recent decades, more than 25 general circulation indices have been produced to define the variability and the long-term change of the EASM. Wang et al. (2008b) arranged the 25 monsoon indices according to their ability to capture the main features of the EASM. The Wang and Fan index (hereafter WF-index; 1999) shows the best performance in capturing the total variance of the precipitation and three-dimensional circulation over East Asia. We, thus, select the WF-index for further analysis. Its definition is a standardised average zonal wind at

850 hPa in (5°-15ºN, 90°-130ºE) minus in (22.5°-32.5ºN, 110°-140ºE). The WF-index is a shear vorticity index which is described by a north-south gradient of the zonal winds. In positive (negative) phase of the WF-index years, two strong (weak) rainfall belts located at the Indo China Peninsula-to-the Philippine Sea and the northern China-to-the Japanese Sea, and a weak (strong) rainfall belt occurs from the Yangtze river basin-to-the south of Japan. The average summer (June-July-August) WF-index is used to represent the EASM for further analysis in this study.

Here, we choose the Niño3.4 and southern oscillation index (SOI) to represent the ENSO status. The Niño3.4 is calculated by the SST anomaly in the central Pacific (190-240ºE, 5ºS-5ºN), while the SOI is based upon the anomaly of the sea level pressure differences between Tahiti (210.75ºE, 17.6ºS) and Darwin (130.83ºE, 12.5ºS). To calculate the SOI, we interpolate the grid data to the Tahiti and the Darwin point by bilinear interpolation.

2.4 METHODS

In this study, we employ the un-centred Pattern Correlation Coefficient (PCC) (for more details see Barnett and Schlesinger, 1987) to analyse the model performance in comparison of the observational data, because centred correlations alone are not sufficient for the attribution of seasonal prediction (Mitchell et al., 2001). The un-centred PCC is defined by:

$$PCC = \frac{\sum_{x=1}^{n}\sum_{y=1}^{m} w_{(x,y)} F_{(x,y)} A_{(x,y)}}{\sqrt{\sum_{x=1}^{n}\sum_{y=1}^{m} w_{(x,y)} F_{(x,y)}^2 \sum_{x=1}^{n}\sum_{y=1}^{m} w_{(x,y)} A_{(x,y)}^2}}$$

where n and m are grids on longitude and latitude, respectively. $F_{(x,y)}$ and $A_{(x,y)}$ represent two dimensions comparison and validating value. $w_{(x,y)}$ indicates the weighting coefficient for each grid. An equal weighting coefficient was applied in the study area.

We also use the anomaly correlation coefficient (ACC) to analyse the model performance in reproducing observational variations. The ACC is the correlation between anomalies of forecasts and those of verifying values with the reference values, such as climatological values (Drosdowsky and Zhang, 2003). Its definition is:

$$ACC = \frac{\sum_{i=1}^{n} w_i (f_i - \bar{f})(a_i - \bar{a})}{\sqrt{\sum_{i=1}^{n} w_i (f_i - \bar{f})^2 \sum_{i=1}^{n} w_i (a_i - \bar{a})^2}}, (-1 \le ACC \le 1)$$

$$f_i = F_i - C_i, \overline{f} = \left(\sum_{i=1}^{n} w_i f_i\right) \Big/ \sum_{i=1}^{n} w_i$$

152

$$a_i = A_i - C_i, \overline{a} = \left(\sum_{i=1}^{n} w_i a_i\right) \Big/ \sum_{i=1}^{n} w_i$$

153

154 where n is the number of samples, and F_i, A_i, C_i represent comparison, verifying value, and
155 reference value such as climatological value, respectively. Also, $\overline{f}$ is the mean of f_i, $\overline{a}$ is the
156 mean of a_i, and w_i indicates the weighting coefficient. If the variation of anomalies of
157 comparison dataset is a coincident with that of the anomalies of verifying value, ACC will
158 take 1 (the maximum value). It indicates that the forecast has good skill.

159 The root-mean-square-error (RMSE) is employed to check the model deviation from the
160 observation and its definition is:

$$RMSE = \sqrt{\sum_{i=1}^{n} w_i D_i^2} \Big/ \sqrt{\sum_{i=1}^{n} w_i}$$

161

162 where D_i represents the deviation between comparison and verifying value, w_i is the
163 weighting coefficient for each sample, and n is the number of samples. If RMSE is closer to
164 zero, it means that the comparisons are closer to the verifying values.

165 ## 3. SEASONAL PREDICTION SKILL OF THE EASM

166 The EASM has complex spatial and temporal structures that encompass the tropics,
167 subtropics, and midlatitudes (Tao and Chen, 1987;Ding, 1994). In the late spring, an
168 enhanced rainfall pattern is observed in the Indochina Peninsula and in the South China Sea.
169 At the same time, the rainfall belt advances northwards to the south of China. In the early
170 summer, the rainfall concentration occurred in the Yangtze River Basin and in southern
171 Japan, namely, the Meiyu and Baiu seasons, respectively. The rainfall belt can reach as far as
172 northern China, the Korean Peninsula (called the Changma rainy season) and central Japan in
173 July (Ding, 2004;Ding and Chan, 2005).

174 The EASM is characterised by both seasonal heterogeneous rainfall distribution and
175 associated large-scale circulation systems (Wang et al., 2008b). In the summer season, water
176 moisture migrates from the Pacific Ocean to central and eastern Asia, which is carried by the

177 southwest surface winds. Generally, a strong summer monsoon year is followed by
178 precipitation in northern China, while a weak summer monsoon year is usually accompanied
179 by heavier rainfall along the Yangtze River basin (Ding, 1994;Zhou and Yu, 2005).

180 For multi-model ensemble mean (MME), the prediction skill of the June-July-August mean
181 rainfall and the associated general circulation variable (*i.e.*, zonal and meridional wind, and
182 mean sea level pressure) is presented in Figure 1. These variables have been widely used to
183 calculate the monsoon index (Wang et al., 2008b). Table 3 shows the contribution of these
184 variables in the EASM. Their abbreviations follow the guidelines of CMIP5 (Taylor et al.,
185 2012). Compared to the non-initialised experiment, a larger predicted area can be found in the
186 initialised experiment, especially for the psl, ua850 and ua200. There are small changes to the
187 predicted area between the non-initialised and initialised experiment for the pr, va850 and
188 va200. The individual model shows an acceptable performance (high PCC) in capturing the
189 observed spatial variation of the six variables, but a poor performance in simulating their
190 temporal variation (with low ACC) (Figure 2). There is no improvement in estimating the
191 spatial variation of the six variables with initialisation. We can see that the models show a
192 higher ACC in the initialised simulations than that in the non-initialised ones. The
193 improvement of simulating the temporal variation of zonal winds (*i.e.*, ua850 and ua200) is
194 larger than that of the rainfall and meridional winds. One can exploit this improvement by
195 using a general circulation based monsoon index as a tool to predict the EASM. As
196 mentioned in section 2.3, the WF-index better represents the monsoon rainfall and its
197 associated general circulation structure than the other monsoon index. Therefore, the
198 prediction skill of EASM in the following analysis is based on the WF-index.

199 In non-initialised simulations, none of the models capture the observed EASM, as indicated
200 by an insignificant ACC (Figure 3). The CanCM4 and the GFDL-CM2p1 simulate a negative
201 phase, while the BCC-CSM1-1, the HadCM3, the MIROC5 and the MPI-ESM-LR all
202 predicted a positive phase of the EASM. With initialisation, the GFDL-CM2p1 and the
203 MIROC5 improve the skill to simulate the EASM, the CanCM4 and the MPI-ESM-LR
204 displayed hardly any reaction, while the BCC-CSM1-1 and the HadCM3 show a worse
205 performance than without initialisation. Particularly with anomaly initialisation, the HadCM3
206 significantly lost its prediction skill in capturing the EASM. The CMIP5 models show
207 different response to the initialisation in predicting the EASM on seasonal time-scale. To

understand the potential reason, we analyse the principle components of six variables, which contribute to the EASM. The details are presented in Section 4.

4. EASM-ENSO COUPLED MODE IN CMIP5

We employ the EOF method to analyse the leading EOF modes of the six meteorological variables anomaly in the EASM region (0°-50ºN, 100°-140ºE). The first EOF mode of the rainfall is characterised by a "sandwich" pattern, which shows sharp contrast between the prominent rainfall centre over Malaysia, the Yangtze River valley and the south of Japan, and the enhanced rainfall over the Indo-China Peninsula and the Philippine Sea (Figure 4). The increased precipitation is associated with cyclones in the low-level (850 hPa) and anti-cyclones in the upper level (200 hPa).

The correlation coefficient of the first eigenvector and the associated principal component (PC) between the model simulation and the observation in the non-initialised and the initialised simulation is presented in Figure 5. Models capture the eigenvector of the first EOF for the six meteorological fields in non-initialised simulation. However, they fail to reproduce the associated PC of the first leading EOF mode. Compared to the non-initialised simulation, models show no improvement to simulate the first leading EOF mode of rainfall, but exhibit a better performance in representing the first leading EOF mode of zonal wind. The CanCM4 and the GFDL-CM2p1 capture the first PC of ua850, but not the other five models. For the zonal wind at 200 hPa, the BCC-CSM1-1 fails to simulate its first EOF mode while the other six models can. Only the GFDL-CM2p1 accurately simulates the first EOF eigenvectors and the associated PC of va850, which cannot be reproduced in the other models. No model captures the spatial-temporal variation of the first EOF mode of meridional wind at 200 hPa. In addition, the GFDL-CM2p1 and the MIROC5 simulate a reasonable leading EOF mode and associated PC of psl, while the other models do not capture it.

Figure 6 shows the fractional (percentage) variances of the six variables from the first EOF mode with the total variances from the observation, and the model simulation with (with-out) initialisation. The observational total variances for the pr, the ua850, the ua200, the va850, the va200 and the psl, are depicted by the first lead EOF mode in 21.2, 59.0, 36.5, 20.6, 28.5 and 50.0 percent, respectively. The prediction systems simulate a comparable explanatory variance, which show a slight discrepancy for the first leading mode in the non-initialisation. From non-initialised simulation to initialised simulation, the prediction systems tend to

enhance the first EOF leading mode because they show larger fractional variances of the total variances of six variables. We note that the CanCM4 and the GFDL-CM2p1 significantly increase the fractional variances from non-initialisation to initialisation.

The ENSO is a dominant mode of the inter-annual variability of the coupled ocean and atmosphere climate system, which has strong effects on the inter-annual variation of the EASM (Wang et al., 2000;Wu et al., 2003). Wang et al. (2015) summarised that the first EOF lead mode of the ASM is ENSO developing mode. As previously mentioned, the first EOF mode is improved in the initialised simulations, compared to the non-initialised simulation. This also can be found in the ENSO indices (Figure 7). The individual members and their ensemble mean of the six models show a low correlation coefficient to the observational Niño3.4 and the SOI in the non-initialised simulations. The two indices show strong anti-phases in the observation, with the correlation range being -0.94 to -0.92 for four seasons (DJF, MAM, JJA, SON). Without initialisation, the models can describe the anti-correlation between Niño3.4 and the SOI, but with a weaker correlation. Compared to the non-initialisation, there is a significant improvement for models in capturing the observation of Niño3.4 and the SOI in the initialised experiments. The initialisation lowers the spread of Niño3.4 and the SOI in all the six models. There is a noticeable change between the model in producing the relationship between the Niño3.4 and the SOI. We find that the GFDL-CM2p1 (HadCM3) shows a lower (higher) Niño3.4-SOI correlation in initialised than that in non-initialised simulations. With initialisation, the ensemble mean of each model outperforms its individual members in capturing Niño3.4 and the SOI, while without initialisation it shows a worse performance than that of the individual members in simulating Niño3.4 and the SOI.

The EASM strongly relies on the pre-seasons ENSO signal due to the lag response of the atmosphere to the SST anomaly (Wu et al., 2003). The lead-lag correlation coefficients between the EASM index and the Niño3.4, and the SOI from JJA(-1) to JJA(+1) are illustrated in Figure 8. The pre-season Niño3.4 (SOI) presents a significant negative (positive) correlation to the EASM, while the post-season Niño3.4 (SOI) shows a notable positive (negative) correlation. This lead-lag correlation coefficient phase is called the Niño3.4-/SOI-EASM coupled mode (Wang et al., 2008b). In the non-initialised cases, the models do not produce the teleconnection between the ENSO and the EASM. The CanCM4, the HadCM3 and the MPI-ESM-LR fail to represent the lead-lag correlation coefficient differences between pre-/post-season ENSO and EASM. The BCC-CSM1-1, the GFDL-

CM2p1 and the MIROC5 capture the coupled mode of the ENSO and the EASM. However, the pre-season ENSO has a weak effect on the EASM. Compared to the non-initialised cases, the MIROC5 and the GFDL-CM2p1 both demonstrate a significant improvement in simulating Niño3.4 (SOI)-EASM coupled mode in the initialisation. The BCC-CSM1-1, the HadCM3, and the HadCM3-ff show no improvement, with insignificant correlation between Niño3.4 (SOI) and the EASM. The CanCM4 and the MPI-ESM-LR indicate a higher correlation between the EASM and the simultaneous-to-post-season ENSO than to the pre-season ENSO.

5. DISCUSSION

The model exhibits a better performance in simulating the general circulation of the EASM with initialisation. Thus, initialisation is helpful in forecasting the EASM on a seasonal time-scale. There are two initialisation methods in our study, full-field initialisation and anomaly initialisation (Table 1). The full-field initialisation produces more skilful predictions on the seasonal time-scale in predicting regional temperature and precipitation (Magnusson et al., 2013;Smith et al., 2013). Nevertheless, for predicting the EASM, there is no significant difference between the two methods. We can see that both the GFDL-CM2p1 and the MIROC5 have significant improvement in capturing the EASM, with full-field and anomaly initialisation, respectively. Only the HadCM3 is initialised by the two initialisation techniques. However, both these two initialised techniques are producing poor predictions of the EASM with no major differences.

The current initialisation strategy updates the observed atmospheric component (*i.e.*, zonal and meridional wind, geopotential height, *etc*.) and the SST (Meehl et al., 2009;Taylor et al., 2012;Meehl et al., 2014). With initialisation, the SST conveys its information via the large heat content of the ocean to the coupled system. Therefore, an index indicating an ocean oscillation like Niño3.4 shows seasonal-to-decadal prediction skill (Jin et al., 2008;Luo et al., 2008;Choi et al., 2016). The models study here demonstrate a prediction skill in simulating Niño3.4 and the SOI due to this effect. The change of the correlation between Niño3.4 and the SOI is insignificant from non-initialised to initialised simulations. We therefore conclude that the relationship between Niño3.4 and the SOI more depends on the model parameterisation than on the initial condition.

Wang *et al*. (2015) found that the second EOF mode of ASM is the Indo-western Pacific monsoon-ocean coupled mode, the third is the Indian Ocean dipole (IOD) mode, and the

fourth is the trend mode. The Indo-western Pacific monsoon-ocean coupled mode is the atmosphere-ocean interaction mode (Wang et al., 2013;Xiang et al., 2013), which is supported by a positive thermodynamic feedback between the western North Pacific (WNP) anticyclone and the underlying Indo-Pacific sea surface temperature anomaly dipole over the warm pool (Wang et al., 2015). The IOD increases the precipitation from the South Asian subcontinent to southeastern China and suppresses the precipitation over the WNP (Wang et al., 2015). It affects the Asian monsoon by the meridional asymmetry of the monsoonal easterly shear during the boreal summer, which can particularly strengthen the northern branch of the Rossby wave response to the south-eastern Indian Ocean SST cooling, leading to an intensified monsoon flow as well as an intensified convection (Wang and Xie, 1996;Wang et al., 2003;Xiang et al., 2011;Wang et al., 2015). We note that the models simulate a reasonable first EOF mode, but illustrate no skill in capturing the other EOF leading modes (not shown). We argue that the models cannot well represent the monsoon-ocean interaction, even with initialisation. The models do not simulate the third EOF leading mode of the EASM since the predictability of the IOD extends only over a three-month time-scale (Choudhury et al., 2015). The current initialisation strategies (both anomaly and full field) enhance the ENSO signal in the model simulations with higher explained fraction of variance. Kim et al. (2012) described a similar finding in ECMWF System 4 and NCEP Climate Forecast System version 2 (CFSv2) seasonal prediction simulations. With initialisation, the models well predict ENSO on seasonal time-scale, which leads to an overly strong modulation of the EASM by ENSO (Jin et al., 2008;Kim et al., 2012).

It is worth mentioning that it is an extremely weak monsoon and strong El Niño year in 1998. The CanCM4, the GFDL-CM2p1, the MIROC5 and the MPI-ESM-LR have the ability to simulate the extreme monsoon event, while the BCC-CSM1-1, and the HadCM3 do not capture it even with initialisation. There is the potential for the BCC-CSM and the HadCM models to improve the teleconnection between the ENSO and the EASM.

This study discusses six CMIP5 models in predicting the EASM on seasonal time-scale. The six models are earth system coupled models which present a better SST-monsoon teleconnection than CMIP3 models (Sperber et al., 2013) and IRI (International Research Institute for Climate and Society) models (Barnston et al., 2010). There are 4 AGCMs contributing to the IRI prediction system, including ECHAM4.5, CCM3.6, COLA and GFDL-AM2p14. These models are forced to forecast the climate on seasonal time-scale by

prescribed SST. Barnston et al. (2010) found that the models showed low prediction skill over East Asia. Therefore, the IRI prediction system cannot be used to predict the EASM. There are two seasonal forecast application systems, the ECMWF System and the NCEP CFS, respectively. Both the two application systems have low prediction skill of EASM (Kim et al., 2012;Jiang et al., 2013). The CMIP5 models have potential to be developed as application system for EASM seasonal prediction, especially the GFDL-CM2p1 and the MIROC5.

To better predict the short-to-long term climate, World Climate Research Programme (WCRP) launched two new projects, i.e., Climate-system Historical Forecast Project (CHFP; Kirtman and Pirani, 2009;Tompkins et al., 2017) and Subseasonal-to-Seasonal (S2S) Prediction Project (Vitart et al., 2017). The two projects coordinate most climate modelling research group and provide a large range of forecast dataset. A comprehensive comparison of all the CHFP and S2S data with the CMIP5 simulations regard to the seasonal prediction skill of the EASM is certainly an interesting topic, which should be addressed in an additional paper.

We have compared six CMIP5 systems with their respective initialisation strategies. The GFDL-CM2p1 and the MIROC5 have the potential to serve as seasonal forecast application system even with their current initialisation method. These models have great potential to optimise the SST-EASM interaction simulation performance to improve their seasonal prediction skill of the EASM.

6. SUMMARY

Six earth system models from CMIP5 have been selected in this study. We have analysed the improvement of the rainfall, the mean sea level pressure, the zonal wind and the meridional wind in the EASM region from non-initialisation to initialisation. The low prediction skill of the summer monsoon precipitation is due to the uncertainties of cloud physics and cumulus parameterisations in the models (Lee et al., 2010;Seo et al., 2015). The models show a better performance in capturing the inter-annual variability of zonal wind than the precipitation with initialisation. Thus, the zonal wind index is an additional factor, which can indicate the prediction skill of the model. When, we calculate the WF-index in both non-initialised and initialised simulations, the GFDL-CM2p1 and the MIROC5 show a significant advancement in simulating the EASM from non-initialised to initialised simulation with a lower RMSE and a higher ACC. There is a slight change in the WF-index calculated from the BCC-CSM1-1,

the CanCM4 and the MPI-ESM-LR data with initialisation. Compared to the non-initialised simulation, the HadCM3 loses prediction skill, especially with anomaly initialisation.

To test the possible mechanisms of the models' performance in the non-initialisation and the initialisation, we have calculated the leading mode of the six fields, which are associated to the EASM. The models demonstrate a better agreement with the observational first EOF mode in the initialised simulations. The first lead mode of zonal wind at 200 hPa show a significant improvement in the models except the BCC-CSM1-1 with initialisation. Therefore, a potential predictor might be an index based upon the zonal wind at 200 hPa. Compared to the non-initialisation, the models enhance the first EOF mode with a higher fraction of variance to the total variance after initialisation. The first EOF mode of the EASM is the ENSO developing mode (Wang et al., 2015). We have analysed the seasonal simulating skill of Niño3.4 and the SOI in each model. The models show a poor performance in representing Niño3.4 and the SOI in the non-initialised simulation. Initialisation improves the model simulating skill of Niño3.4 and the SOI. The initialised simulations decrease the spread of ensemble members in the models. We find that there is no significant change in the models reproducing the correlation between Niño3.4 and the SOI from non-initialisation to initialisation.

In general, the pre-season warm phase of the ENSO (El Niño) leads to a weak EASM producing more rainfall over the South China Sea and northwest China, and less rainfall over the Yangtze River Valley and the southern Japan; the cold phase of the ENSO (La Niña) illustrated a reverse rainfall pattern to El Niño in East Asia. The pre-season Niño3.4 (SOI) exhibits a strong negative (positive) correlation to the EASM, while the correlation between the post-season Niño3.4 (SOI) and the EASM illustrated an anti-phase as the pre-season. In the non-initialised simulations, the models do not capture Niño3.4-/SOI-EASM coupled mode. The MIROC5 is the only one model has the ability to represent the Niño3.4-EASM coupled mode with initialisation. For the SOI-EASM coupled mode, the GFDL-CM2p1 and the MIROC5 capture it in the initialisation, while the BCC-CSM1-1, the HadCM3, the HadCM2-ff, the CanCM4 and the MPI-ESM-LR do not. Therefore, we argue that the differential depiction of ENSO-EASM coupled mode in CMIP5 models lead to their differential response to initialisation.

Acknowledgements

The China Scholarship Council (CSC) and the Freie Universität Berlin supported this work. We would like to thank the climate modelling groups listed in Table 1 of this paper for producing and making their model output available. We acknowledge the MiKlip project funded by the Federal Ministry of Education and Research and the German Climate Computing Centre (DKRZ) and the HPC Service of ZEDAT for providing the data services. We are grateful to Mrs Margerison Patricia for her useful comments and the proofreading work on this manuscript. Authors thank two anonymous reviewers for their useful inputs to the manuscript.

References

Adler, R. F., Huffman, G. J., Chang, A., Ferraro, R., Xie, P.-P., Janowiak, J., Rudolf, B., Schneider, U., Curtis, S., Bolvin, D., Gruber, A., Susskind, J., Arkin, P., and Nelkin, E.: The Version-2 Global Precipitation Climatology Project (GPCP) Monthly Precipitation Analysis (1979–Present), J Hydrometeorol, 4, 1147-1167, 10.1175/1525-7541(2003)004<1147:tvgpcp>2.0.co;2, 2003.

Arora, V. K., Scinocca, J. F., Boer, G. J., Christian, J. R., Denman, K. L., Flato, G. M., Kharin, V. V., Lee, W. G., and Merryfield, W. J.: Carbon emission limits required to satisfy future representative concentration pathways of greenhouse gases, Geophys Res Lett, 38, L05805, 10.1029/2010gl046270, 2011.

Barnett, T. P., and Schlesinger, M. E.: Detecting Changes in Global Climate Induced by Greenhouse Gases, J Geophys Res Atmos, 92, 14772-14780, 10.1029/JD092iD12p14772, 1987.

Barnston, A. G., Li, S. H., Mason, S. J., DeWitt, D. G., Goddard, L., and Gong, X. F.: Verification of the First 11 Years of IRI's Seasonal Climate Forecasts, J Appl Meteorol Clim, 49, 493-520, 10.1175/2009jamc2325.1, 2010.

Choi, J., Son, S. W., Ham, Y. G., Lee, J. Y., and Kim, H. M.: Seasonal-to-Interannual Prediction Skills of Near-Surface Air Temperature in the CMIP5 Decadal Hindcast Experiments, J Clim, 29, 1511-1527, 10.1175/Jcli-D-15-0182.1, 2016.

Choudhury, D., Sharma, A., Sivakumar, B., Sen Gupta, A., and Mehrotra, R.: On the predictability of SSTA indices from CMIP5 decadal experiments, Environ Res Lett, 10, 074013, 10.1088/1748-9326/10/7/074013, 2015.

Dee, D. P., Uppala, S. M., Simmons, A. J., Berrisford, P., Poli, P., Kobayashi, S., Andrae, U., Balmaseda, M. A., Balsamo, G., Bauer, P., Bechtold, P., Beljaars, A. C. M., van de Berg, L., Bidlot, J., Bormann, N., Delsol, C., Dragani, R., Fuentes, M., Geer, A. J., Haimberger, L., Healy, S. B., Hersbach, H., Holm, E. V., Isaksen, L., Kallberg, P., Kohler, M., Matricardi, M., McNally, A. P., Monge-Sanz, B. M., Morcrette, J. J., Park, B. K., Peubey, C., de Rosnay, P., Tavolato, C., Thepaut, J. N., and Vitart, F.: The ERA-Interim reanalysis: configuration and performance of the data assimilation system, Q J R Meteorolog Soc, 137, 553-597, 10.1002/qj.828, 2011.

Delworth, T. L., Broccoli, A. J., Rosati, A., Stouffer, R. J., Balaji, V., Beesley, J. A., Cooke, W. F., Dixon, K. W., Dunne, J., Dunne, K. A., Durachta, J. W., Findell, K. L., Ginoux, P., Gnanadesikan, A., Gordon, C. T., Griffies, S. M., Gudgel, R., Harrison, M. J., Held, I. M., Hemler, R. S., Horowitz, L. W., Klein, S. A., Knutson, T. R., Kushner, P. J., Langenhorst, A. R., Lee, H. C., Lin, S. J., Lu, J., Malyshev, S. L., Milly, P. C. D., Ramaswamy, V., Russell, J.,

Schwarzkopf, M. D., Shevliakova, E., Sirutis, J. J., Spelman, M. J., Stern, W. F., Winton, M., Wittenberg, A. T., Wyman, B., Zeng, F., and Zhang, R.: GFDL's CM2 global coupled climate models. Part I: Formulation and simulation characteristics, J Clim, 19, 643-674, 10.1175/Jcli3629.1, 2006.
Ding, Y.: Seasonal march of the East-Asian summer monsoon., in: East Asian Monsoon, edited by: Chang, C.-P., World Scientific, Singapore, 560, 2004.
Ding, Y. H.: Monsoons over China, Kluwer Academic Publisher, Dordrecht/Boston/London, 419 pp., 1994.
Ding, Y. H., and Chan, J. C. L.: The East Asian summer monsoon: an overview, Meteorol Atmos Phys, 89, 117-142, 10.1007/s00703-005-0125-z, 2005.
Drosdowsky, W., and Zhang, H.: Verification of Spatial Fields, in: Forecast Verification: A Practitioner's Guide in Atmospheric Science edited by: Jolliffe, L. T., and Stephenson, D. B., John Wiley & Sons Ltd, England, 128-129, 2003.
Goddard, L., Mason, S. J., Zebiak, S. E., Ropelewski, C. F., Basher, R., and Cane, M. A.: Current approaches to seasonal-to-interannual climate predictions, Int J Climatol, 21, 1111-1152, 10.1002/joc.636, 2001.
Huang, B. Y., Banzon, V. F., Freeman, E., Lawrimore, J., Liu, W., Peterson, T. C., Smith, T. M., Thorne, P. W., Woodruff, S. D., and Zhang, H. M.: Extended Reconstructed Sea Surface Temperature Version 4 (ERSST.v4). Part I: Upgrades and Intercomparisons, J Clim, 28, 911-930, 10.1175/Jcli-D-14-00006.1, 2015.
Jiang, X. W., Yang, S., Li, Y. Q., Kumar, A., Liu, X. W., Zuo, Z. Y., and Jha, B.: Seasonal-to-Interannual Prediction of the Asian Summer Monsoon in the NCEP Climate Forecast System Version 2, J Clim, 26, 3708-3727, 10.1175/Jcli-D-12-00437.1, 2013.
Jin, E. K., Kinter, J. L., Wang, B., Park, C. K., Kang, I. S., Kirtman, B. P., Kug, J. S., Kumar, A., Luo, J. J., Schemm, J., Shukla, J., and Yamagata, T.: Current status of ENSO prediction skill in coupled ocean–atmosphere models, Clim Dyn, 31, 647-664, 10.1007/s00382-008-0397-3, 2008.
Kang, I.-S., and Shukla, J.: Dynamic seasonal prediction and predictability of the monsoon, in: The Asian Monsoon, edited by: Wang, B., Springer Berlin Heidelberg, Berlin, Heidelberg, 585-612, 2006.
Kang, I. S., and Yoo, J. H.: Examination of multi-model ensemble seasonal prediction methods using a simple climate system, Clim Dyn, 26, 285-294, 10.1007/s00382-005-0074-8, 2006.
Kim, H. J., Wang, B., and Ding, Q. H.: The Global Monsoon Variability Simulated by CMIP3 Coupled Climate Models, J Clim, 21, 5271-5294, 10.1175/2008jcli2041.1, 2008.
Kim, H. J., Takata, K., Wang, B., Watanabe, M., Kimoto, M., Yokohata, T., and Yasunari, T.: Global Monsoon, El Nino, and Their Interannual Linkage Simulated by MIROC5 and the CMIP3 CGCMs, J Clim, 24, 5604-5618, 10.1175/2011jcli4132.1, 2011.
Kim, H. M., Webster, P. J., Curry, J. A., and Toma, V. E.: Asian summer monsoon prediction in ECMWF System 4 and NCEP CFSv2 retrospective seasonal forecasts, Clim Dyn, 39, 2975-2991, 10.1007/s00382-012-1470-5, 2012.
Kirtman, B., and Pirani, A.: The State of the Art of Seasonal Prediction Outcomes and Recommendations from the First World Climate Research Program Workshop on Seasonal Prediction, Bull Am Meteorol Soc, 90, 455-458, 10.1175/2008bams2707.1, 2009.
Kug, J. S., Kang, I. S., and Choi, D. H.: Seasonal climate predictability with Tier-one and Tier-two prediction systems, Clim Dyn, 31, 403-416, DOI 10.1007/s00382-007-0264-7, 2008.
Lee, J.-Y., Wang, B., Kang, I. S., Shukla, J., Kumar, A., Kug, J. S., Schemm, J. K. E., Luo, J. J., Yamagata, T., Fu, X., Alves, O., Stern, B., Rosati, T., and Park, C. K.: How are seasonal

prediction skills related to models' performance on mean state and annual cycle?, Clim Dyn, 35, 267-283, 10.1007/s00382-010-0857-4, 2010.
Luo, J.-J., Masson, S., Behera, S. K., and Yamagata, T.: Extended ENSO Predictions Using a Fully Coupled Ocean–Atmosphere Model, J Clim, 21, 84-93, 10.1175/2007jcli1412.1, 2008.
Magnusson, L., Alonso-Balmaseda, M., Corti, S., Molteni, F., and Stockdale, T.: Evaluation of forecast strategies for seasonal and decadal forecasts in presence of systematic model errors, Clim Dyn, 41, 2393-2409, 10.1007/s00382-012-1599-2, 2013.
Matei, D., Pohlmann, H., Jungclaus, J., Muller, W., Haak, H., and Marotzke, J.: Two Tales of Initializing Decadal Climate Prediction Experiments with the ECHAM5/MPI-OM Model, J Clim, 25, 8502-8523, 10.1175/Jcli-D-11-00633.1, 2012.
Meehl, G., Covey, C., Delworth, T., Latif, M., McAvaney, B., Mitchell, J., Stouffer, R., and Taylor, K.: The WCRP CMIP3 multi-model dataset: a new era in climate change research, Bull Am Meteorol Soc, 88, 1383-1394, 2007.
Meehl, G. A., Goddard, L., Murphy, J., Stouffer, R. J., Boer, G., Danabasoglu, G., Dixon, K., Giorgetta, M. A., Greene, A. M., Hawkins, E., Hegerl, G., Karoly, D., Keenlyside, N., Kimoto, M., Kirtman, B., Navarra, A., Pulwarty, R., Smith, D., Stammer, D., and Stockdale, T.: DECADAL PREDICTION Can It Be Skillful?, Bull Am Meteorol Soc, 90, 1467-1485, 10.1175/2009bams2778.1, 2009.
Meehl, G. A., and Teng, H. Y.: Case studies for initialized decadal hindcasts and predictions for the Pacific region, Geophys Res Lett, 39, L22705, 10.1029/2012gl053423, 2012.
Meehl, G. A., Goddard, L., Boer, G., Burgman, R., Branstator, G., Cassou, C., Corti, S., Danabasoglu, G., Doblas-Reyes, F., Hawkins, E., Karspeck, A., Kimoto, M., Kumar, A., Matei, D., Mignot, J., Msadek, R., Navarra, A., Pohlmann, H., Rienecker, M., Rosati, T., Schneider, E., Smith, D., Sutton, R., Teng, H. Y., van Oldenborgh, G. J., Vecchi, G., and Yeager, S.: DECADAL CLIMATE PREDICTION An Update from the Trenches, Bull Am Meteorol Soc, 95, 243-267, 10.1175/Bams-D-12-00241.1, 2014.
Mitchell, J. F. B., Karoly, D. J., Hegerl, G. C., Zwiers, F. W., Allen, M. R., and Marengo, J.: Detection of Climate Change and Attribution of Causes, in: Third Assessment Report of the Intergovernmental Panel on Climate Change., edited by: Houghton, J. T., Griggs, D. J., Noguer, M., van der Linden, P. J., Dai, X., Maskell, K., and Johnson, C. A., Cambridge University Press, New York, 470, 2001.
Seo, K. H., Son, J. H., Lee, J. Y., and Park, H. S.: Northern East Asian Monsoon Precipitation Revealed by Airmass Variability and Its Prediction, J Clim, 28, 6221-6233, 10.1175/Jcli-D-14-00526.1, 2015.
Smith, D. M., Eade, R., and Pohlmann, H.: A comparison of full-field and anomaly initialization for seasonal to decadal climate prediction, Clim Dyn, 41, 3325-3338, 10.1007/s00382-013-1683-2, 2013.
Sperber, K., Annamalai, H., Kang, I. S., Kitoh, A., Moise, A., Turner, A., Wang, B., and Zhou, T.: The Asian summer monsoon: an intercomparison of CMIP5 vs. CMIP3 simulations of the late 20th century, Clim Dyn, 41, 2711-2744, 10.1007/s00382-012-1607-6, 2013.
Sperber, K. R., Brankovic, C., Deque, M., Frederiksen, C. S., Graham, R., Kitoh, A., Kobayashi, C., Palmer, T., Puri, K., Tennant, W., and Volodin, E.: Dynamical seasonal predictability of the Asian summer monsoon, Mon Weather Rev, 129, 2226-2248, 10.1175/1520-0493(2001)129<2226:Dspota>2.0.Co;2, 2001.
Tao, S. Y., and Chen, L. X.: A review of recent research on the East Asian summer monsoon in China, in: Monsoon Meterology, edited by: Chang, C.-P., and Krishnamurti, T. N., Oxford University Press, Oxford, 60-92, 1987.
Tatebe, H., Ishii, M., Mochizuki, T., Chikamoto, Y., Sakamoto, T. T., Komuro, Y., Mori, M., Yasunaka, S., Watanabe, M., Ogochi, K., Suzuki, T., Nishimura, T., and Kimoto, M.: The

539 Initialization of the MIROC Climate Models with Hydrographic Data Assimilation for
540 Decadal Prediction, J Meteorol Soc Japan, 90a, 275-294, 10.2151/jmsj.2012-A14, 2012.
541 Taylor, K. E., Stouffer, R. J., and Meehl, G. A.: An Overview of CMIP5 and the Experiment
542 Design, Bull Am Meteorol Soc, 93, 485-498, 10.1175/Bams-D-11-00094.1, 2012.
543 Tompkins, A. M., Ortiz De Zarate, M. I., Saurral, R. I., Vera, C., Saulo, C., Merryfield, W. J.,
544 Sigmond, M., Lee, W. S., Baehr, J., Braun, A., Butler, A., Deque, M., Doblas-Reyes, F. J.,
545 Gordon, M., Scaife, A. A., Imada, Y., Ishii, M., Ose, T., Kirtman, B., Kumar, A., Muller, W.
546 A., Pirani, A., Stockdale, T., Rixen, M., and Yasuda, T.: The Climate-System Historical
547 Forecast Project: Providing Open Access to Seasonal Forecast Ensembles from Centers
548 around the Globe, Bull Am Meteorol Soc, 98, 2293-2302, 10.1175/Bams-D-16-0209.1, 2017.
549 Vitart, F., Ardilouze, C., Bonet, A., Brookshaw, A., Chen, M., Codorean, C., Deque, M.,
550 Ferranti, L., Fucile, E., Fuentes, M., Hendon, H., Hodgson, J., Kang, H. S., Kumar, A., Lin,
551 H., Liu, G., Liu, X., Malguzzi, P., Mallas, I., Manoussakis, M., Mastrangelo, D., MacLachlan,
552 C., McLean, P., Minami, A., Mladek, R., Nakazawa, T., Najm, S., Nie, Y., Rixen, M.,
553 Robertson, A. W., Ruti, P., Sun, C., Takaya, Y., Tolstykh, M., Venuti, F., Waliser, D.,
554 Woolnough, S., Wu, T., Won, D. J., Xiao, H., Zaripov, R., and Zhang, L.: The Subseasonal to
555 Seasonal (S2s) Prediction Project Database, Bull Am Meteorol Soc, 98, 163-+,
556 10.1175/Bams-D-16-0017.1, 2017.
557 Wang, B., and Xie, X.: Low-Frequency Equatorial Waves in Vertically Sheared Zonal Flow.
558 Part I: Stable Waves, J Atmos Sci, 53, 449-467, 10.1175/1520-
559 0469(1996)053<0449:lfewiv>2.0.co;2, 1996.
560 Wang, B., and Fan, Z.: Choice of south Asian summer monsoon indices, Bull Am Meteorol
561 Soc, 80, 629-638, 10.1175/1520-0477(1999)080<0629:Cosasm>2.0.Co;2, 1999.
562 Wang, B., Wu, R. G., and Fu, X. H.: Pacific-East Asian teleconnection: how does ENSO
563 affect East Asian climate?, J Clim, 13, 1517-1536, 2000.
564 Wang, B., Wu, R., and Li, T.: Atmosphere–Warm Ocean Interaction and Its Impacts on
565 Asian–Australian Monsoon Variation*, J Clim, 16, 1195-1211, 10.1175/1520-
566 0442(2003)16<1195:aoiaii>2.0.co;2, 2003.
567 Wang, B., Kang, I.-S., and Lee, J.-Y.: Ensemble Simulations of Asian–Australian Monsoon
568 Variability by 11 AGCMs*, J Clim, 17, 803-818, 10.1175/1520-
569 0442(2004)017<0803:esoamv>2.0.co;2, 2004.
570 Wang, B., Ding, Q. H., Fu, X. H., Kang, I. S., Jin, K., Shukla, J., and Doblas-Reyes, F.:
571 Fundamental challenge in simulation and prediction of summer monsoon rainfall, Geophys
572 Res Lett, 32, L15711, 10.1029/2005gl022734, 2005.
573 Wang, B.: The Asian Monsoon, Springer Science & Business Media, Praxis, New York, NY,
574 USA, 2006.
575 Wang, B., Lee, J.-Y., Kang, I.-S., Shukla, J., Park, C. K., Kumar, A., Schemm, J., Cocke, S.,
576 Kug, J. S., Luo, J. J., Zhou, T., Wang, B., Fu, X., Yun, W. T., Alves, O., Jin, E. K., Kinter, J.,
577 Kirtman, B., Krishnamurti, T., Lau, N. C., Lau, W., Liu, P., Pegion, P., Rosati, T., Schubert,
578 S., Stern, W., Suarez, M., and Yamagata, T.: Advance and prospectus of seasonal prediction:
579 assessment of the APCC/CliPAS 14-model ensemble retrospective seasonal prediction
580 (1980–2004), Clim Dyn, 33, 93-117, 10.1007/s00382-008-0460-0, 2008a.
581 Wang, B., Wu, Z. W., Li, J. P., Liu, J., Chang, C. P., Ding, Y. H., and Wu, G. X.: How to
582 measure the strength of the East Asian summer monsoon, J Clim, 21, 4449-4463,
583 10.1175/2008jcli2183.1, 2008b.
584 Wang, B., Xiang, B., and Lee, J. Y.: Subtropical high predictability establishes a promising
585 way for monsoon and tropical storm predictions, Proc Natl Acad Sci U S A, 110, 2718-2722,
586 10.1073/pnas.1214626110, 2013.

Wang, B., Lee, J. Y., and Xiang, B. Q.: Asian summer monsoon rainfall predictability: a predictable mode analysis, Clim Dyn, 44, 61-74, 10.1007/s00382-014-2218-1, 2015.
Wu, R. G., Hu, Z. Z., and Kirtman, B. P.: Evolution of ENSO-related rainfall anomalies in East Asia, J Clim, 16, 3742-3758, 10.1175/1520-0442(2003)016<3742:Eoerai>2.0.Co;2, 2003.
Wu, T. W., Song, L. C., Li, W. P., Wang, Z. Z., Zhang, H., Xin, X. G., Zhang, Y. W., Zhang, L., Li, J. L., Wu, F. H., Liu, Y. M., Zhang, F., Shi, X. L., Chu, M., Zhang, J., Fang, Y. J., Wang, F., Lu, Y. X., Liu, X. W., Wei, M., Liu, Q. X., Zhou, W. Y., Dong, M., Zhao, Q. G., Ji, J. J., Li, L., and Zhou, M. Y.: An Overview of BCC Climate System Model Development and Application for Climate Change Studies, J Meteorol Res-Prc, 28, 34-56, 10.1007/s13351-014-3041-7, 2014.
Wu, Z. W., Wang, B., Li, J. P., and Jin, F. F.: An empirical seasonal prediction model of the east Asian summer monsoon using ENSO and NAO, J Geophys Res Atmos, 114, D18120, 10.1029/2009jd011733, 2009.
Xiang, B., Wang, B., Yu, W., and Xu, S.: How can anomalous western North Pacific Subtropical High intensify in late summer?, Geophys Res Lett, 40, 2349-2354, 10.1002/grl.50431, 2013.
Xiang, B. Q., Yu, W. D., Li, T., and Wang, B.: The critical role of the boreal summer mean state in the development of the IOD, Geophys Res Lett, 38, L02710, 10.1029/2010gl045851, 2011.
Yang, S., Zhang, Z. Q., Kousky, V. E., Higgins, R. W., Yoo, S. H., Liang, J. Y., and Fan, Y.: Simulations and seasonal prediction of the Asian summer monsoon in the NCEP Climate Forecast System, J Clim, 21, 3755-3775, 10.1175/2008jcli1961.1, 2008.
Yim, S. Y., Wang, B., and Xing, W.: Prediction of early summer rainfall over South China by a physical-empirical model, Clim Dyn, 43, 1883-1891, 10.1007/s00382-013-2014-3, 2014.
Zhou, T., Wu, B., and Wang, B.: How Well Do Atmospheric General Circulation Models Capture the Leading Modes of the Interannual Variability of the Asian–Australian Monsoon?, J Clim, 22, 1159-1173, 10.1175/2008jcli2245.1, 2009.
Zhou, T. J., and Yu, R. C.: Atmospheric water vapor transport associated with typical anomalous summer rainfall patterns in China, J Geophys Res Atmos, 110, D08104, 10.1029/2004jd005413, 2005.

619 Table 1. Details of the prediction systems investigated in this study.

System	Institute	Resolution		Non-Initialisation	Initialisation		Reference
		Atmospheric	Oceanic	Members	Members	Type	
BCC-CSM1-1	Beijing Climate Center, China	T42L26	1lonx1.33lat L40	3	3	Full-field	Wu *et al*. (2014)
CanCM4	Canadian Centre for Climate Modelling and Analysis, Canada	T63L35	256 x 192 L40	10	10	Full-field	Arora *et al*. (2011)
GFDL-CM2p1	Geophysical Fluid Dynamics Laboratory, USA	N45L24	1lon x 0.33-1lat L50	10	10	Full-field	Delworth *et al*. (2006)
HadCM3	Met Office Hadley Centre, UK	N48L19	1.25x1.25 L20	10	10 + 10	Full-field and Anomaly	Smith *et al*. (2013)
MIROC5	Atmosphere and Ocean Research Institute, Japan	T85L40	256x192 L44	5	6	Anomaly	Tatebe *et al*. (2012)
MPI-ESM-LR	Max Planck Institute for Meteorology, Germany	T63L47	GR15 L40	3	3	Anomaly	Matei *et al*. (2012)

620

Table 2. Brief summaries of initialisation strategies used by modelling groups in the study. ECMWF: European Centre for Medium-Range Weather Forecasts; GODAS: Global Ocean Data Assimilation System; NCEP: National Centers for Environmental Prediction; S: Salinity; SODA: Simple Ocean Data Assimilation; T: Temperature. Initialised date shows the first initialised day of every prediction year.

system	Atmosphere	Ocean	Initialised date	Internet
BCC-CSM1-1	-	integration with ocean T nudged to SODA product above 1500 m	Ensemble 1: 1st September Ensemble 2: 1st November Ensemble 3: 1st January	http://forecast.bcccsm.ncc-cma.net/
CanCM4	ECMWF re-analysis	off-line assimilation of SODA and GODAS subsurface ocean T and S adjusted to reserve model T-S	1st January	http://www.cccma.ec.gc.ca/
GFDL-CM2p1	GFDL re-analysis	assimilates observations of T, S from World Ocean Database	1st January	https://www.gfdl.noaa.gov/multidecadal-prediction-stream/
HadCM3	ECMWF re-analysis	off-line ocean re-analysis product	1st November	http://cerawww.dkrz.de/WDCC/CMIP5/
MIROC5	-	integration using observational gridded ocean T and S	1st January	http://amaterasu.ees.hokudai.ac.jp/
MPI-ESM-LR	NCEP re-analysis	off-line ocean hindcast forced with NCEP	1st January	http://cerawww.dkrz.de/WDCC/CMIP5/

628 Table 3. Description of the six variables which contribute to the EASM. The abbreviation of these variables is followed to the guidelines of CMIP5.

variable	Standard name	Contribution to the EASM
pr	Precipitation	Precipitation distribution indicates the strength of EASM
psl	Mean sea surface pressure	Differences of mean sea surface pressure between land and ocean lead to EASM
ua850	Zonal winds over 850 hPa	A component of low-level cyclone which transports vapor from ocean to land
va850	Meridional winds over 850 hPa	As ua850, and contributes to Hadley's cell
va200	Meridional winds over 850 hPa	A component of upper-level Hadley's cell
ua200	Zonal winds over 850 hPa	As va200

629

630

631

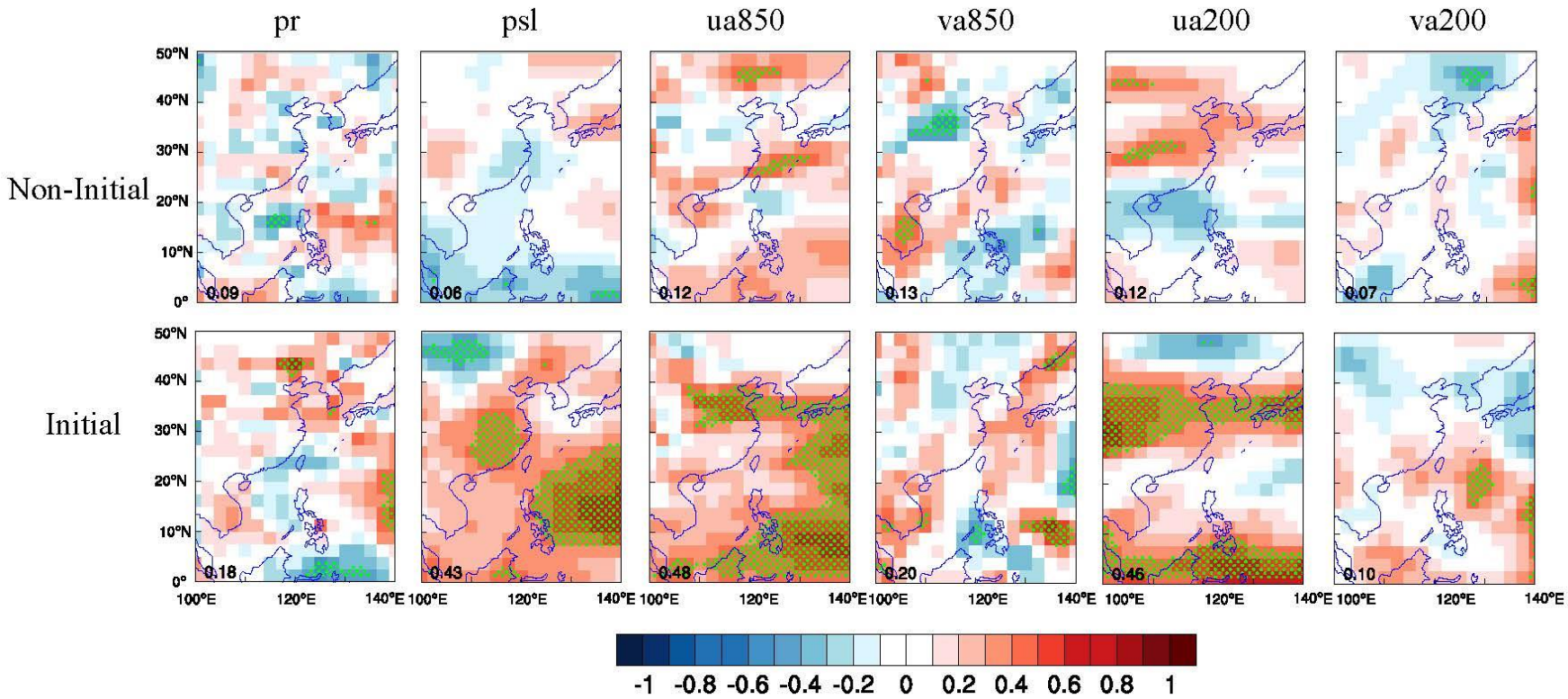

Fig. 1. Anomaly correlation coefficient of six variables (i.e. precipitation, mean sea level pressure, and winds over 850 hPa and 200 hPa) between multi-model ensemble mean and observations in non-initialisation and initialisation. The green dotted grids illustrate the significant level at 0.05. The number at lower left corner indicates the ratio of significant grid points to entire grids. The GPCP is employed as the reference data for precipitation (pr) while winds (i.e. ua850, va850, ua200 and va200) and mean sea level pressure (psl) are compared with ERA-Interim re-analysis.

637

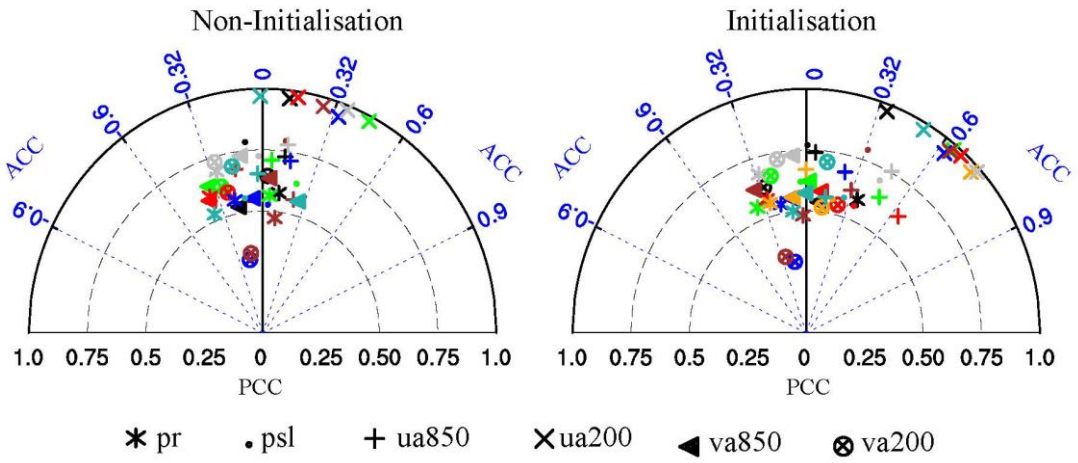

638

639 Fig.2. Taylor diagrams display of pattern (PCC) and temporal (ACC) correlation
640 metrics of six variables between observation and model simulation in the EASM
641 region (0-50ºN, 100-140ºE). Each coloured marker represents a model, *i.e.*, the BCC-
642 CSM1-1 (black), the CanCM4 (green), the GFDL-CM2p1 (red), the HadCM3 (blue),
643 the MIROC5 (brown), the MPI-ESM-LR (light-sea-blue), and the HadCM3-ff
644 (orange).

645

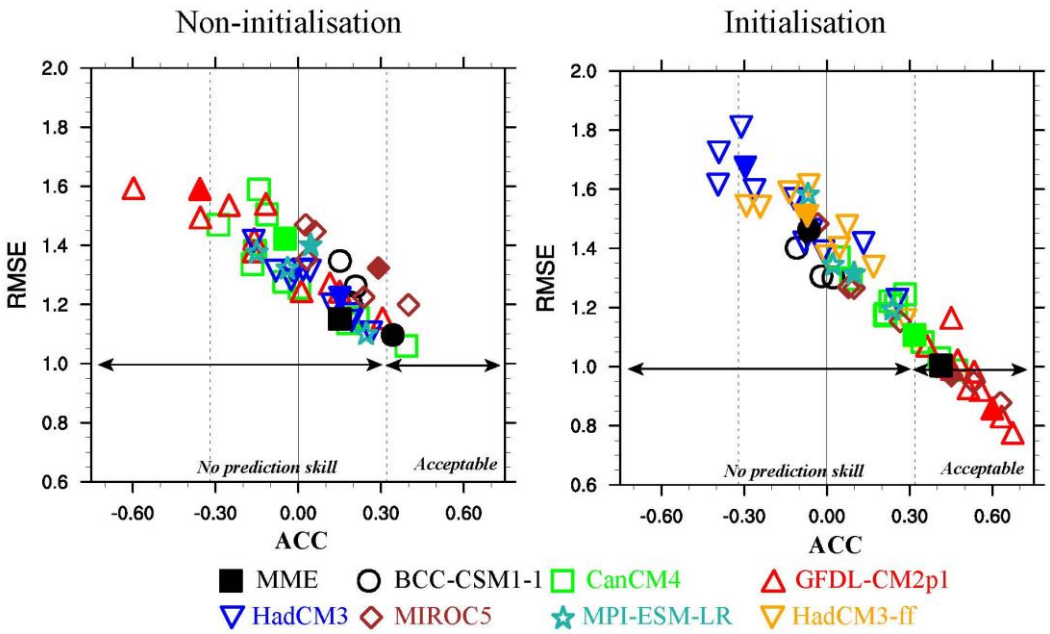

Fig. 3. Performance of the model ensemble member (hollow marker) and its ensemble mean (solid marker) on the EASM index. The abscissa and ordinates are the anomaly correlation coefficient (ACC) and the root-mean-square-error (RMSE), respectively. The observation of EASM index is calculated by zonal wind at 850 hPa from the ERA-Interim re-analysis data. The black dot lines indicate the significant level at 0.1. The vertical black line represents the correlation between the simulation and the observation of EASM index is 0.

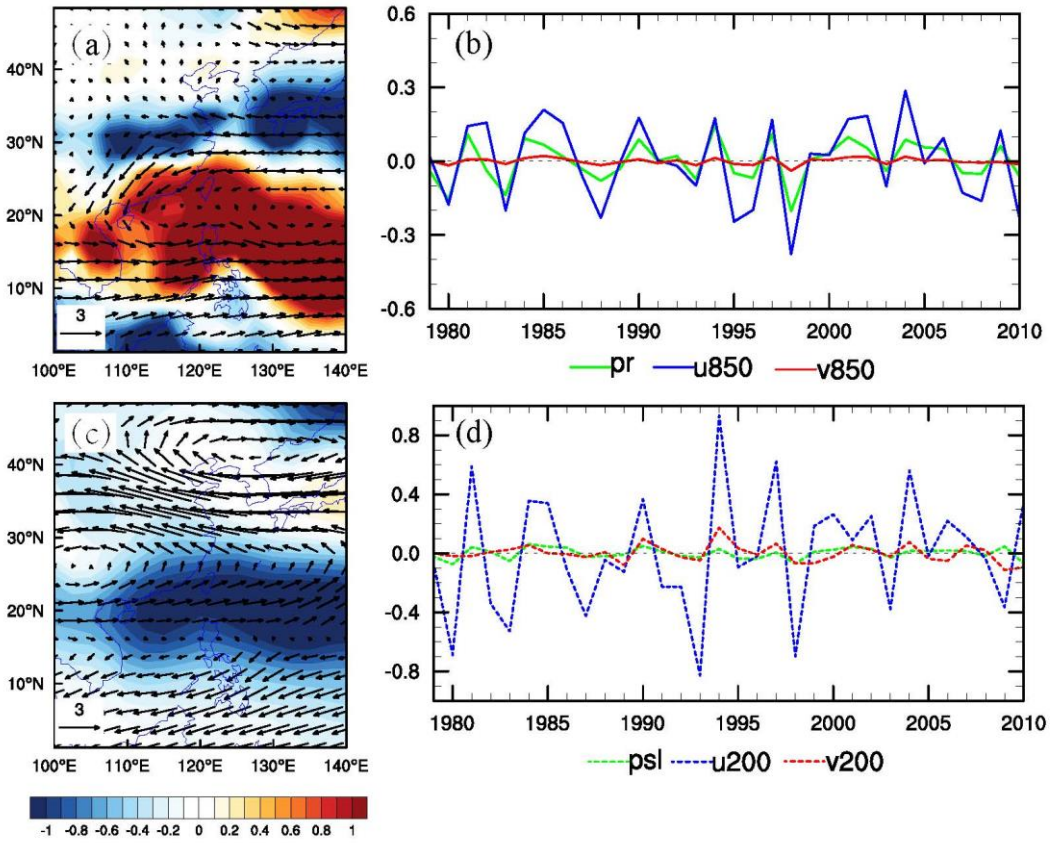

Fig. 4. Spatial distribution of the first leading EOF mode of June-July-August precipitation and winds over 850 hPa (a), mean sea level pressure and winds over 200 hPa (c) and the associated principal component (PC; b, d). The GPCP and the ERA-Interim data from 1979-2005 are used for the EOF analysis in the EASM domain.

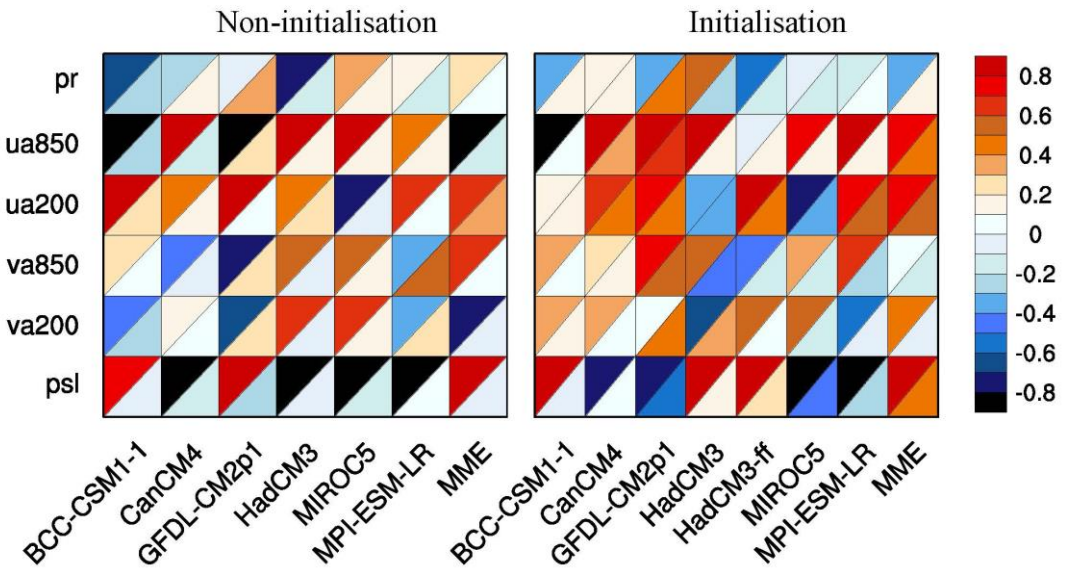

Fig. 5. Portrait diagram display of correlation metrics between the observation and the model simulation of the first lead EOF mode for the six fields in the non-initialisation (left) and the initialisation (right). Each grid square is split by a diagonal in order to show the correlation with respect to both the eigenvector (upper left triangle) and its associated principal components (lower right triangle) reference data sets.

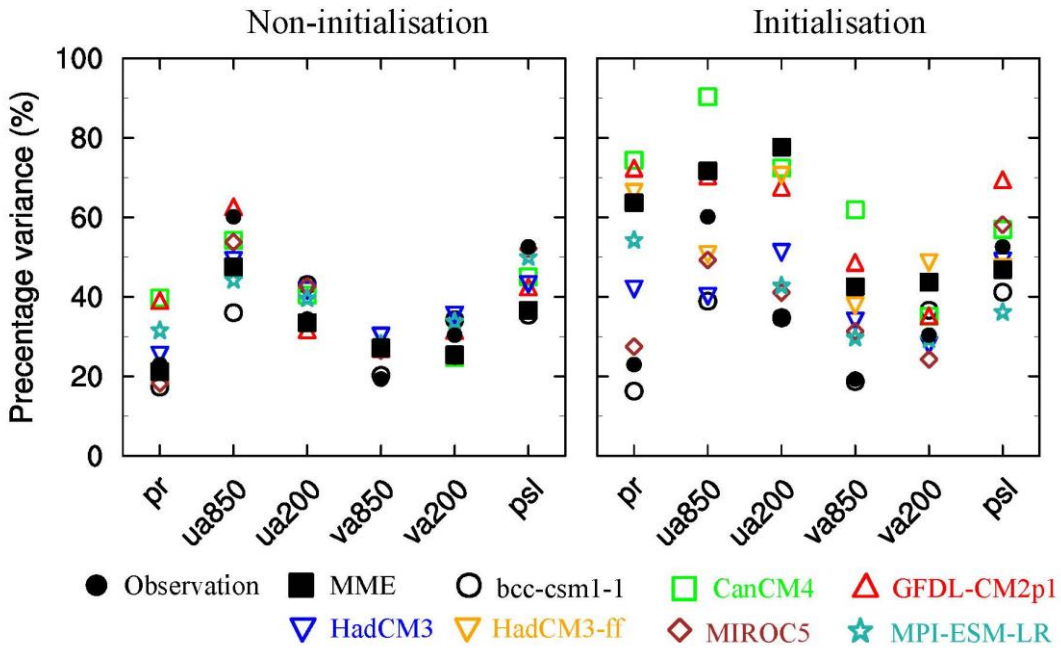

Fig. 6. Fraction variance (%) explained by the first EOF mode for six fields in the non-initialisation (left) and the initialisation (right).

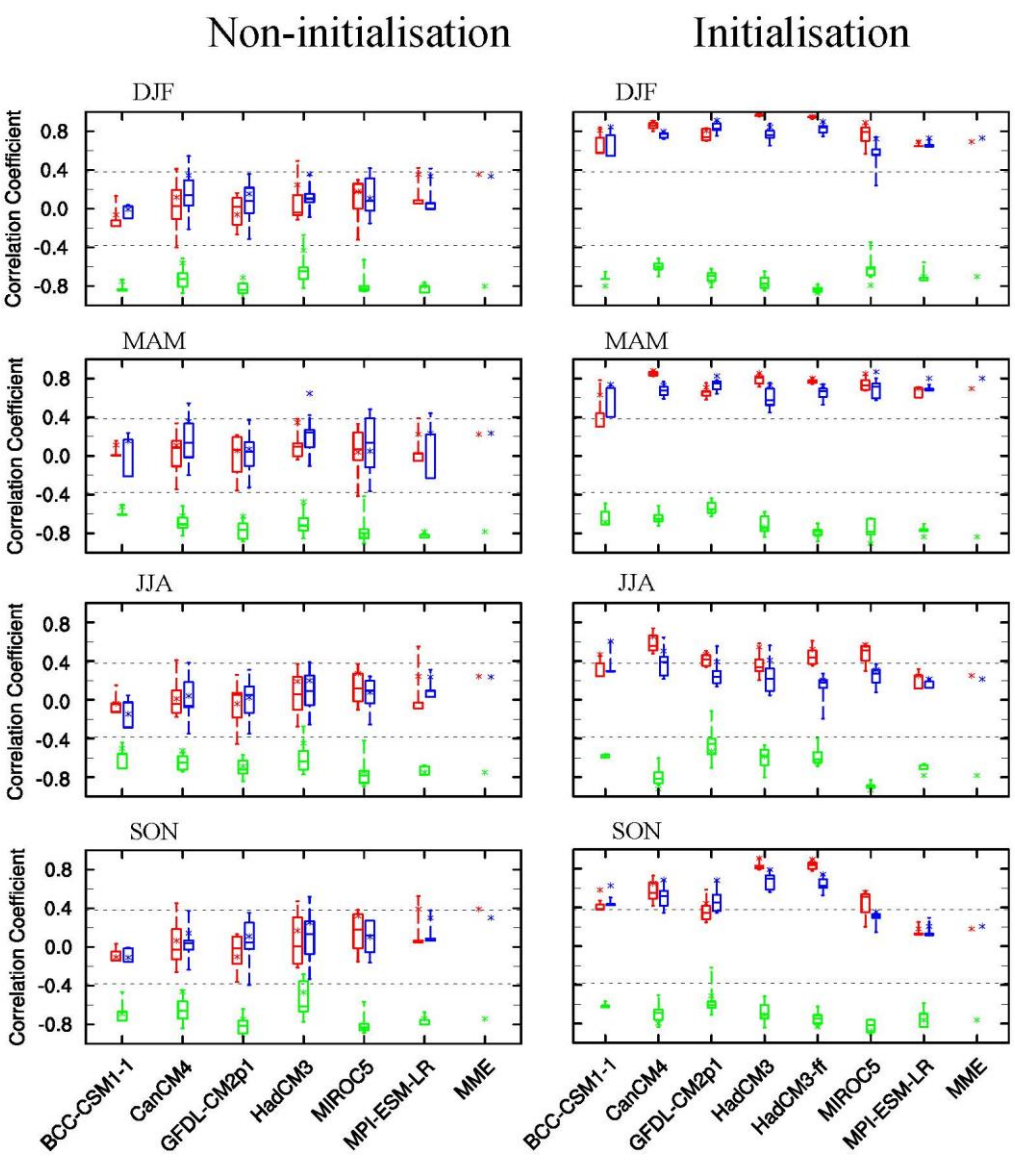

675

676 Fig. 7. Model prediction skill of Niño3.4 (red), SOI (blue) from DJF to SON in non-
677 initialised (left) and initialised (right) simulations. Green diagrams show the
678 correlation coefficient between the model simulation of Niño3.4 and the SOI. Box and
679 whisker diagrams show ensemble mean of each model (asterisk), median (horizontal
680 line), 25th and 75th percentiles (box), minimum and maximum (whisker). The two
681 black dotted lines indicate 0.05 significant level based upon Student's t-test.

682

683

684

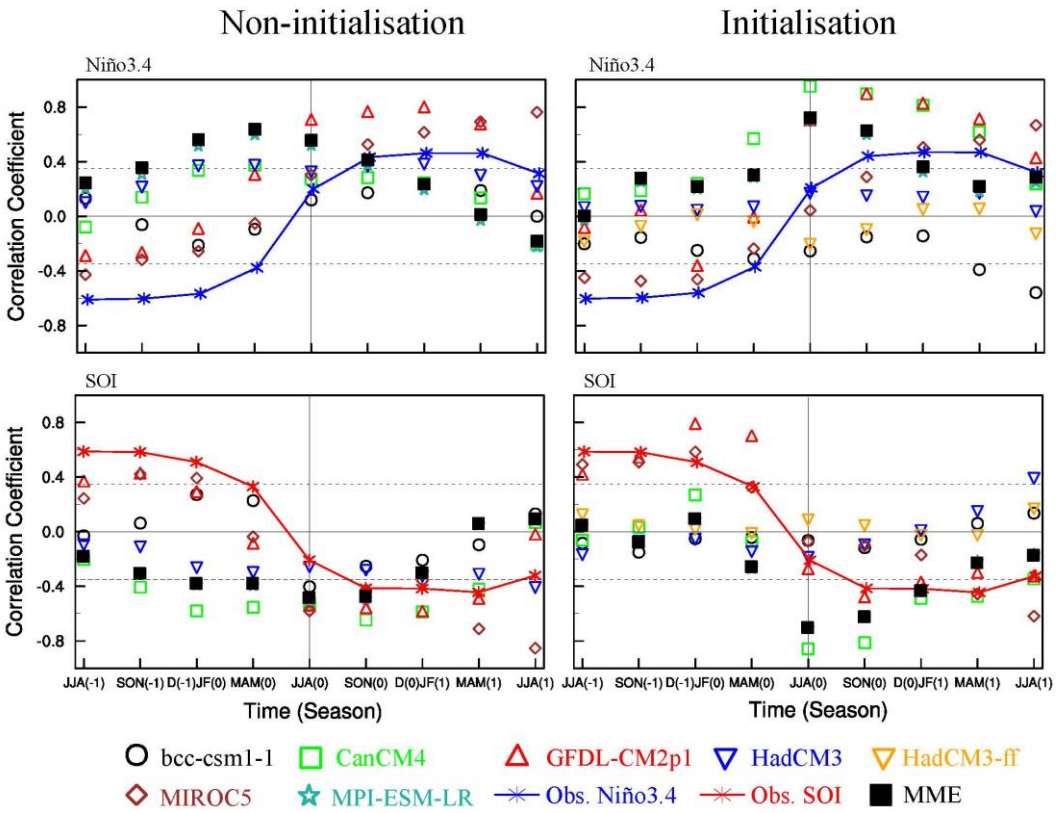

Fig. 8. Lead-lag correlation coefficients between the EASM index and Niño3.4 (upper), and SOI (lower) in non-initialised simulations (left) and initialised ones (right) for observation (marker line) and models (marker) from JJA(-1) to JJA(+1). The two black dotted lines are 0.05 significant level based upon Student's t-test. The vertical line represents JJA(0), where the simultaneous correlations between the EASM index and Niño3.4, and SOI are shown.